Materials Research Letters

ISSN: 2166-3831 (Online) Journal homepage: www.tandfonline.com/journals/tmrl20

Rendering $Ti_3C_2T_x$ (MXene) monolayers visible

A. Miranda, J. Halim, A. Lorke & M. W. Barsoum

To cite this article: A. Miranda, J. Halim, A. Lorke & M. W. Barsoum (2017) Rendering $Ti_3C_2T_x$ (MXene) monolayers visible, Materials Research Letters, 5:5, 322-328, DOI: 10.1080/21663831.2017.1280707

To link to this article: https://doi.org/10.1080/21663831.2017.1280707

© 2017 The Author(s). Published by Informa UK Limited, trading as Taylor & Francis Group.

Published online: 01 Feb 2017.

Submit your article to this journal

Article views: 6074

View related articles

View Crossmark data

Citing articles: 19 View citing articles

Full Terms & Conditions of access and use can be found at
https://www.tandfonline.com/action/journalInformation?journalCode=tmrl20

MATER. RES. LETT., 2017
VOL. 5, NO. 5, 322–328
http://dx.doi.org/10.1080/21663831.2017.1280707

MATERIALS RESEARCH LETTERS
Taylor & Francis
Taylor & Francis Group

ORIGINAL REPORT

OPEN ACCESS

Rendering $Ti_3C_2T_x$ (MXene) monolayers visible

A. Miranda[a], J. Halim[b], A. Lorke[a] and M. W. Barsoum[b]

[a]Department of Physics and CENIDE, Universität Duisburg-Essen, Duisburg, Germany; [b]Department of Materials Science and Engineering, Drexel University, Philadelphia, PA, USA

ABSTRACT

Herein we report on how to render $Ti_3C_2T_x$ (MXene) monolayers deposited on SiO_2/Si wafers, with different SiO_2 thicknesses, visible. Inputting the effective thickness of a $Ti_3C_2T_x$ monolayer (1 ± 0.2 nm) measured by atomic force microscopy, and its refractive index into a Fresnel-law-based simulation software, we show that the optical contrast of $Ti_3C_2T_x$ monolayers deposited on SiO_2/Si wafers depends on the SiO_2 thickness, number of MXene layers, and the light's wavelength. The highest contrast was found for SiO_2 thicknesses around 220 nm. Simulations for other substrates, namely, Al_2O_3/Si, HfO_2/Si, Si_3N_4/Si and Al_2O_3/Al, are presented as supplementary information.

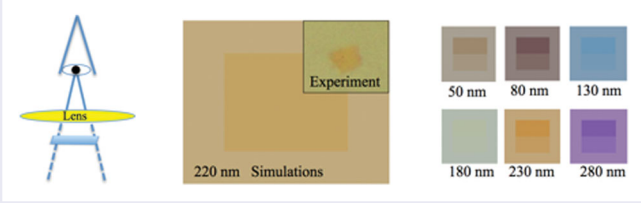

IMPACT STATEMENT

The experimental and simulated color contrasts between $Ti_3C_2T_x$ (MXene) monoflakes deposited on SiO_2 of various thicknesses—under an optical microscope—were obtained for the first time.

ARTICLE HISTORY
Received 7 October 2016

KEYWORDS
Optical microscope; optical properties; MXene monolayers; visibility

Introduction

Recent years have seen an increasing interest in the study of 2D materials and their practical applications [1–3] both alone or in stacked configurations [4,5]. This interest was catalyzed by a 2004 paper on graphene [6], and now extends toward other 2D materials such as boron nitride (BN) [7], transition metal dichalcogenides [8–10], and black phosphorous [11], among others.

MXenes—early transition metal carbides and/or nitrides, that are produced by the selective etching of the A layers from the MAX phases—represent the newest, and potentially largest, 2D family of solids [12–15]. The MAX phases, in turn, are a large (>70) family of layered ternary transition metal carbides, where M is an early transition metal, A is an A-group element (mostly groups 13 and 14), and X is C or/and N [16]. Because during etching, the A-group element layers such as Al and Ga are replaced by –O, –OH, and –F terminations [17,18], the proper designation of the resulting 2D material is $M_{n+1}C_nT_x$, where T represents a surface termination, which can be O, OH, and/or F [17].

The most studied MXene to date is $Ti_3C_2T_x$, which has already shown potential for use in a number of diverse applications, such as batteries [19,20], supercapacitors [21,22], fuel cells [23], sensors [24,25], transparent conducting electrodes [26,27], photocatalytic applications [28], and water treatment [29] among others [30–33]. Most, if not all, of the aforementioned work has been carried out on multilayers and/or films, both thick and thin.

Recently, we reported on electric transport in single, free-standing isolated $Ti_3C_2T_x$ monolayers where we showed that at $\approx 1 \times 10^{28}\ m^{-3}$, the density of mobile carriers in this material is quite high [34]. Even more recently, we reported on conductive transparent spin-coated $Ti_3C_2T_x$ films, with high figures of merit [27]. During the course of that work, both the real, n, and imaginary, k, optical constants of these spincast films

CONTACT M. W. Barsoum barsoumw@drexel.edu Department of Materials Science and Engineering, Drexel University, Philadelphia, PA19104, USA

Supplemental data for this article can be accessed here. http://dx.doi.org/10.1080/21663831.2017.1280707

© 2017 The Author(s). Published by Informa UK Limited, trading as Taylor & Francis Group.
This is an Open Access article distributed under the terms of the Creative Commons Attribution License (http://creativecommons.org/licenses/by/4.0/), which permits unrestricted use, distribution, and reproduction in any medium, provided the original work is properly cited.

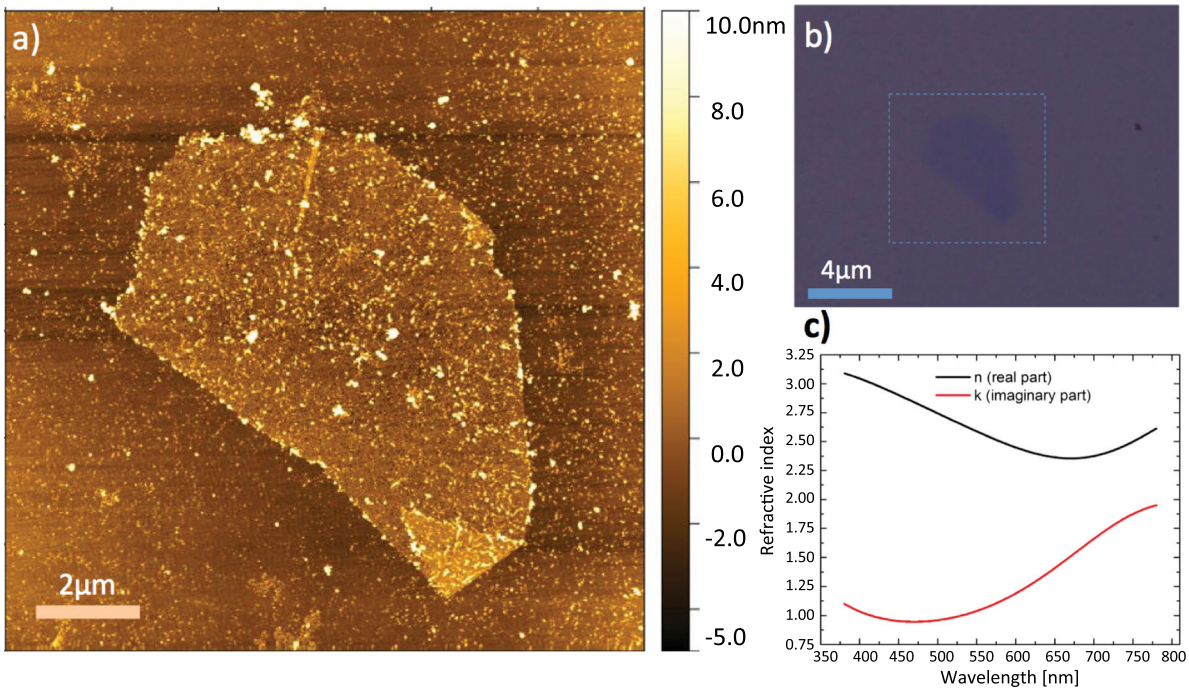

Figure 1. (a) AFM scan of a $Ti_3C_2T_x$ monolayer on a 285 nm thick SiO_2 substrate. Average height between flake and substrate is 1.8 ± 0.3 nm. AFM measurements of the folded corner are more reliable as they are less influenced by instrumental offsets and other artifacts. These measurements show a reproducible step of 1 ± 0.2 nm, which is the value assumed herein. Small bright regions in (a) are residues from the MXene dispersion; (b) visible spectrum unfiltered OM images of same flake—located in the center of the dotted frame—in which the folded MXene corner appears slightly darker. (c) Ellipsometric measurements of the real, *n*, and imaginary, *k*, parts of the refractive indices of $Ti_3C_2T_x$ as a function of wavelength in the visible region, reproduced from Ref. [27].

were measured [27]. Since as discussed below, *n* and *k* are important input parameters in our modeling, it is important to briefly explain how they were measured and why it is justifiable to use these values here. First, both single flakes and films were spincast from nominally identical colloidal solutions. Second, given that *n* and *k* are typically functions of film thickness, it would have been ideal if the values used herein were those measured on monolayered films. However, since currently such films do not exist, we chose instead to use the *n* and *k* values (Figure 1(c)), measured ellipsometrically on a 75 nm thick spincoated $Ti_3C_2T_x$ film. The details can be found in supplementary information of Ref. [27].

As far as we are aware, that information has yet to be exploited to render MXenes visible under an optical microscope (OM), in the same way that, for example, Blake et al. [35] and others [36–39], rendered single graphene layers visible. The same was done for single layers of transition metal dichalcogenides [40], BN [41], and other 2D systems [42]. The capability to quickly and accurately distinguish single from multiple flakes is a crucial requisite first step for using MXenes in microelectronic devices. To be able to do so rapidly and accurately with nothing more sophisticated than an OM is therefore important. The purpose of this work is to delineate the conditions under which $Ti_3C_2T_x$ monolayers, deposited on oxidized Si wafers, would be visible under an OM. To that effect, we measured the thicknesses of various flakes—deposited on substrates with varying SiO_2 thicknesses—using atomic force microscopy (AFM). We then combined these results, with the refractive indices of $Ti_3C_2T_x$ [27], to predict the best conditions to visualize $Ti_3C_2T_x$ monoflakes in an OM for a variety of substrates.

The $Ti_3C_2T_x$ flakes were produced by selective etching of Al from Ti_3AlC_2. The details can be found elsewhere [34]. To deposit single $Ti_3C_2T_x$ flakes, they were first dispersed in water—with a concentration of ≈ 1 to 2 mg/ml—and spincoated on Si wafers. For the latter, a drop was placed on the substrate and the spincoater was accelerated from 0 to 6000 rpm in 1 s and held at that speed for 60 s. The substrates were then inspected under an OM. Flakes, presumed to be monolayers, were scanned by tapping mode AFM. The difference in height between the monolayers and the Si substrate was measured to be 1.8 ± 0.3 nm, which overestimates the real thickness because of anomalies related to the measuring conditions of the AFM [43], instrument offset [44], and

other artifacts [45,46], as well as the possible presence of adsorbates on top of the flakes in addition to surface terminations. The same is true of graphene where control experiments on monolayered graphene flakes revealed them to be offset by about ≈ 0.6 nm under the same experimental and environmental conditions. To solve this problem, the 2D community has concluded that folded regions give the most reliable measurements of thickness (see, e.g. [47]). Measurements on folded flakes here provided a reproducible thickness of 1 ± 0.2 nm, for a $Ti_3C_2T_x$ monolayer, in agreement with the SiO_2-MXene step height (1.8 ± 0.3 nm) reduced by the determined offset of ≈ 0.6 nm. It is important to note that, based on X-ray diffraction measurements, half the c-axis lattice parameter of $Ti_3C_2T_x$ is ≈ 1 nm [12]. Therefore, all such flakes were deemed single-layered.

Figure 1(a) shows the AFM scan for a monolayer MXene flake deposited on a Si wafer with a nominally 300 nm thick SiO_2 layer. In the AFM scan shown in Figure 1(a), small particulates are imaged both on the MXene and substrate. These particulates are most probably small oxide particles that form during MXene production and need further investigation. The largest of these particles are detectable under an OM and have been avoided when selecting regions for colorimetric evaluations. An OM micrograph taken using the whole range of visible light is shown in Figure 1(b).

Figure 1(c) shows the functional dependencies of n and k of $Ti_3C_2T_x$, on wavelength, λ, in the visible range (380–780 nm), which is the region of interest for this work. These values are taken from Ref. [27] and are reproduced here because the colorimetric simulations are based on them. Interestingly, we note that the average values of n and k in this region (2.6 and 1.3) are comparable to those of graphene in the same spectral window [48,49].

Similar to what was done for other 2D systems [35,40], we model our MXene sample as a stacked structure (Figure 2(a)) composed of air (layer 0, with refractive index n_0), MXene (layer 1, with thickness d_1 and refractive index n_1), SiO_2 (layer 2, with thickness d_2 and refractive index n_2 [50,51], and Si (layer 3, with refractive index n_3 [52]. Under these conditions, the MXene reflectivity is given by [53]:

$$R_{\mathrm{MXene}} = \left| \frac{r_1\, e^{i(\phi_1+\phi_2)} + r_2\, e^{-i(\phi_1-\phi_2)} + r_3\, e^{-i(\phi_1+\phi_2)} + r_1 r_2 r_3\, e^{i(\phi_1-\phi_2)}}{e^{i(\phi_1+\phi_2)} + r_1 r_2\, e^{-i(\phi_1-\phi_2)} + r_1 r_3\, e^{-i(\phi_1+\phi_2)} + r_2 r_3\, e^{i(\phi_1-\phi_2)}} \right|^2, \tag{1}$$

where $r_1 = (n_0 - n_1)/(n_0 + n_1)$, $r_2 = (n_1 - n_2)/(n_1 + n_2)$, and $r_3 = (n_2 - n_3)/(n_2 + n_3)$ are the relative changes in the index of refraction and $\phi_i = 2\pi n_i d_i/\lambda$ are the phase shifts in the various regions of the optical path for a given λ. Similarly, the substrate without

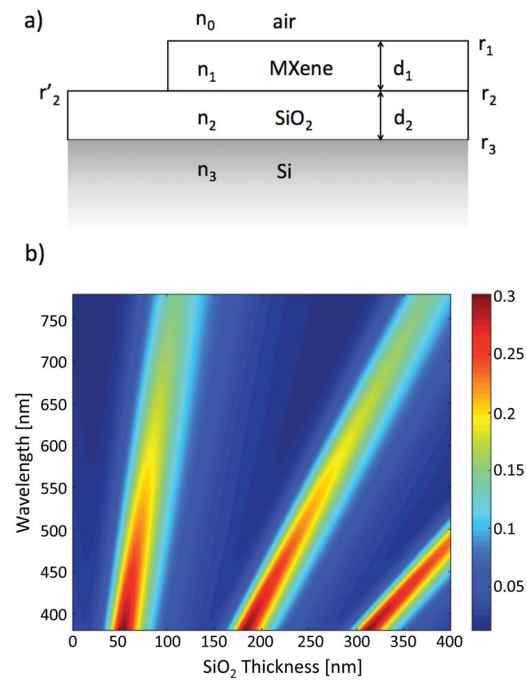

Figure 2. (a) Schematic of simulated MXene/SiO_2/Si trilayer modeled. (b) Color plot of the contrast as a function of SiO_2 thickness and λ for $Ti_3C_2T_x$ monolayers. Note the strong dependence on both λ and SiO_2 thickness. Three regions with high contrast can be easily seen. These regions delineate the best experimental conditions for the visualization of a $Ti_3C_2T_x$ monolayer. The color scale on the right shows the expected contrast.

MXene has a reflectivity expressed by $R_{\mathrm{Sub}} = |(r_2'\, e^{i\phi_2} + r_3\, e^{-i\phi_2})/(e^{i\phi_2} + r_2' r_3\, e^{-i\phi_2})|^2$, where $r_2' = (n_0 - n_2)/(n_0 + n_2)$. The absolute contrast for a MXene monolayer for a given λ is defined as:

$$C = \left| \frac{R_{\mathrm{MXene}} - R_{\mathrm{Sub}}}{R_{\mathrm{MXene}}} \right|. \tag{2}$$

When this equation is plotted for a single $Ti_3C_2T_x$ layer as a function of SiO_2 thickness and λ (Figure 2(b)), three regions of high contrast are found. These represent the optimal experimental conditions for the identification of single $Ti_3C_2T_x$ layers on SiO_2. They roughly follow the relation $2 \cdot d_{SiO_2} \cdot n_{SiO_2} = (m + 1/2)\lambda$, with $m = 0, 1, 2$, corresponding to the optical path being a half-integer times the wavelength. This formula indicates that these Fabry-Perot-type resonances come from standing waves in the SiO_2 and reflection at an open end (antinode) on the MXene-SiO_2 interface side and reflection at a fixed end (node) on the Si–SiO_2 interface side. Figure 3(a–c) show the contrast between 1 (bottom curve) to 5 (top curve) layers of $Ti_3C_2T_x$ as a function of SiO_2 thickness for monochromatic blue, green, and red light, respectively. Note that the position of the absolute contrast maxima for each λ is independent of the number of MXene layers.

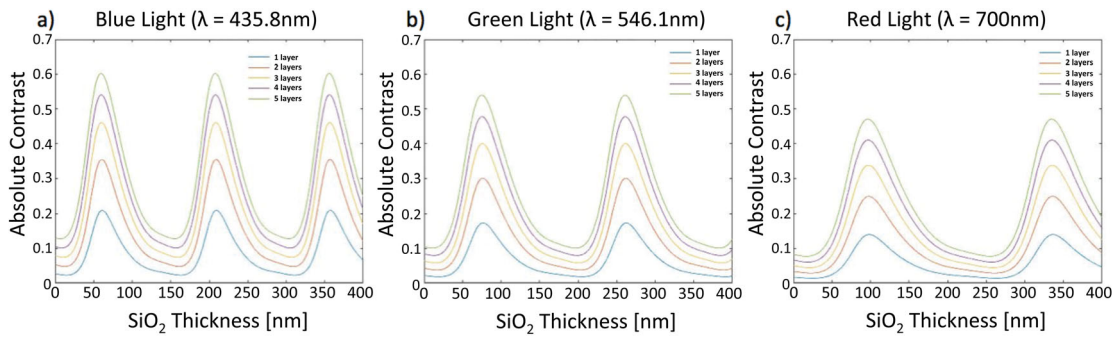

Figure 3. Color plot of the absolute contrast as a function of SiO_2 thickness for 1–5 $Ti_3C_2T_x$ layers predicted for, (a) blue (435.8 nm), (b) green (546.1 nm), and (c) red (700 nm) light. The contrast maxima vary for each λ, but are not functions of the number of MXene layers.

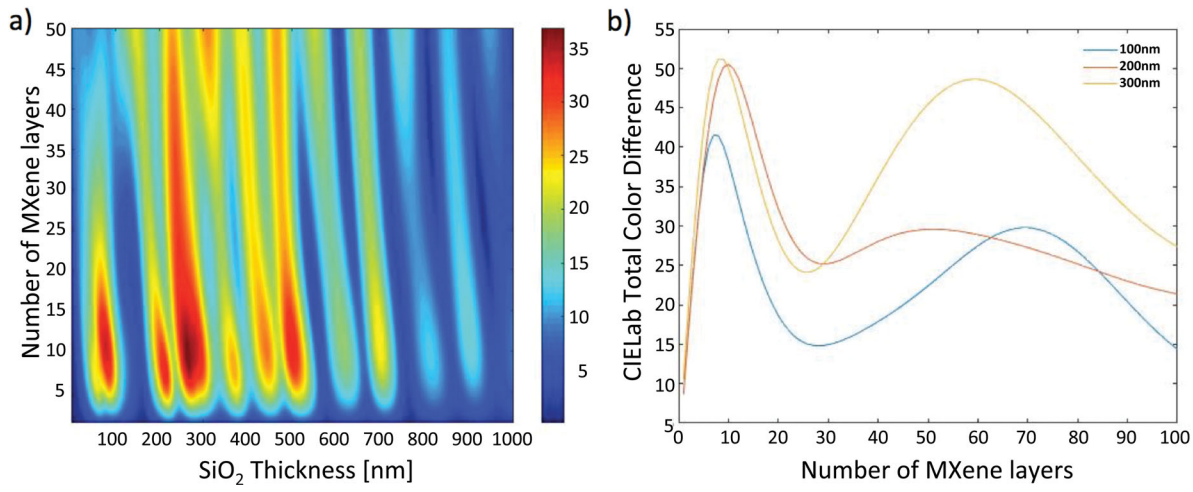

Figure 4. (a) Color plot of contrast between SiO_2 and $Ti_3C_2T_x$ monolayers as a function of the number of the latter and the thickness of the former observed under a tungsten lamp delineating the experimental conditions for which the contrast would be greatest; (b) Contrast difference as a function of 1–100 $Ti_3C_2T_x$ layers for three different SiO_2 thicknesses. Contrast depends on number of $Ti_3C_2T_x$ monolayers and peaks around 8–12 layers. For the thickest SiO_2 layer, a second maximum is seen around 60 layers. Herein each monolayer is assumed to be 1 nm.

Since these results pertain to a single λ, they are not of much use in an OM without filters, where all frequencies need to be taken into account. In that case, the colorimetric CIE 1931 XYZ [54] space should be calculated for visible wavelengths as:

$$\begin{pmatrix} X_j \\ Y_j \\ Z_j \end{pmatrix} = P \int_{380\,\mathrm{nm}}^{780\,\mathrm{nm}} S(\lambda) R(\lambda) \begin{pmatrix} \bar{x}(\lambda) \\ \bar{y}(\lambda) \\ \bar{z}(\lambda) \end{pmatrix} \mathrm{d}\lambda \qquad (3)$$

where $\bar{x}(\lambda)$, $\bar{y}(\lambda)$, and $\bar{z}(\lambda)$ are the CIE 1931 matching functions, respectively (See Ref. [54] for selected colorimetric tables), $R(\lambda)$ is the reflectivity of the system, $S(\lambda)$ is the spectrum of the incident light source, that depends on the type of illumination and P is the total illumination power. The incident light source used here is an incandescent tungsten-filament light with a temperature of 2856 K, the most common source of light in OMs and thus illuminant A is used. It is described by a Planck's distribution law (shown in the supplementary information (SI)) and tabulated in Ref. [54]. Once the CIE 1931 XYZ color space is calculated, it is transformed to the CIELab color space which offers a more perceptual uniformity [39,54], by operating the transformations [39]:

$$L^* = 116 f\left(\frac{Y}{Y_n}\right) - 16, \quad a^* = 500\left[f\left(\frac{X}{X_n}\right) - f\left(\frac{Y}{Y_n}\right)\right],$$
$$b^* = 200\left[f\left(\frac{Y}{Y_n}\right) - f\left(\frac{Z}{Z_n}\right)\right], \qquad (4)$$

where X_n, Y_n, and Z_n are the coordinates for the white point of the reference illuminant (109.850, 100, and 35.585, respectively, in case of illuminant A) and

$$f = \begin{cases} t^{1/3} & \text{if } t > (6/29)^3 \\ \frac{1}{3}(29/6)^2 t + \frac{4}{29} & \text{otherwise} \end{cases}. \qquad (5)$$

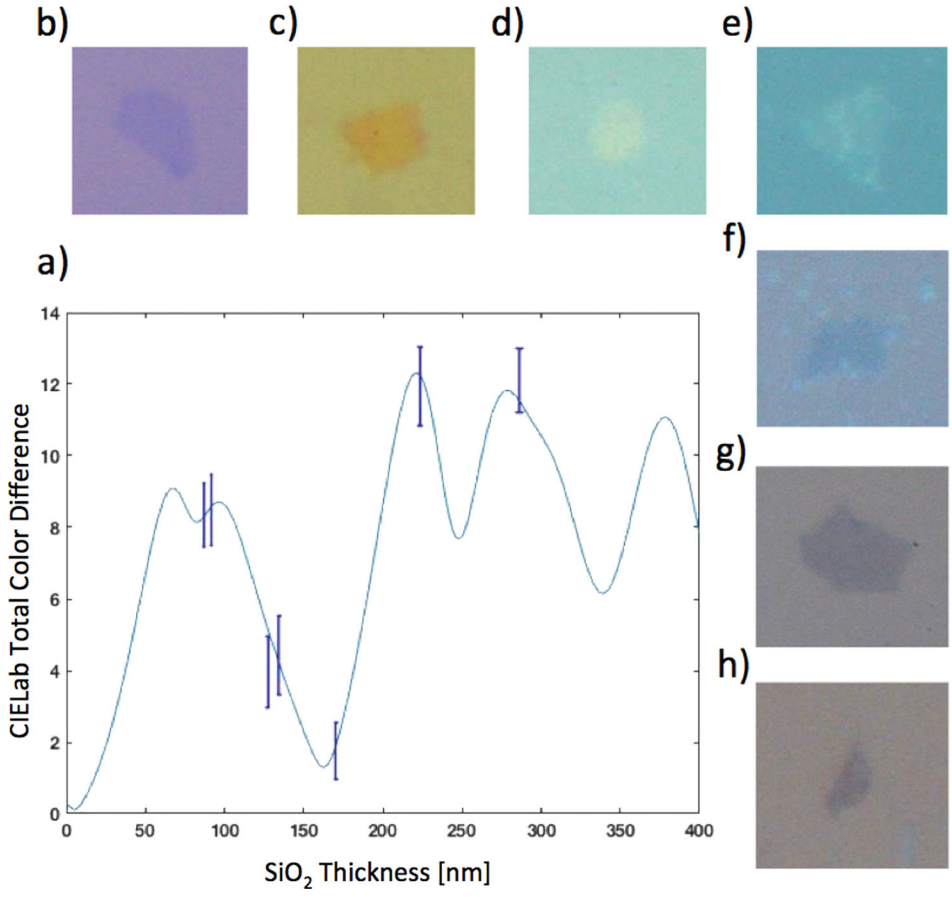

Figure 5. (a) Total color difference of a Ti3C2T*x* monolayer as a function of the SiO_2 layer thickness. Error bars represent experimental values for samples with the corresponding SiO_2 thicknesses. (b–h) OM images of Ti_3C_2Tx monolayers on SiO_2 with thicknesses of 285, 223, 170, 134, 127, 90, and 87 nm, respectively, to which the data points in (a) correspond. All micrographs have dimension of $20 \times 20\ \mu m^2$. Flakes were illuminated by a standard W-lamp, without filters under the same experimental and environmental conditions (clean room controlled temperature and humidity). The luminosity of these pictures was adjusted in order to have a consistent color balance between experiment and simulations [38]. The experimentally measured CIELab total color differences are in quite good agreement with the calculations.

Lastly, we use the total color difference, TCD, defined as

$$\mathrm{TCD}_{\mathrm{CIE76}} = \sqrt{(\Delta L^*)^2 + (\Delta a^*)^2 + (\Delta b^*)^2}, \quad (6)$$

as the colorimetric distance between two colors.

Figure 4(a) shows the calculated color contrast between bare and $Ti_3C_2T_x$ covered substrates as a function of the number of monolayers—up to 50—and the thickness of the SiO_2, observed under a W-lamp (Illuminant A), delineating the experimental conditions for which the contrast would be largest. Here again there are combinations of the number of layers and SiO_2 thicknesses that result in bands of high contrast. When the same results are plotted as a function of the number of MXene layers—for three different SiO_2 thicknesses, 100, 200, and 300 nm (Figure 4(b))—the contrast curves have maxima between 8 and 12 layers before decreasing. Interestingly, there is second peak—at around 60 layers for the thickest SiO_2 substrates—possibly a Fabry-Perot resonance in the MXene layer.

Since herein we were particularly interested in identifying single flakes, Figure 5(a) plots the color contrast for the latter as a function of SiO_2 thickness. These results predict that a SiO_2 thickness of 222 nm provides the highest contrast. To test this prediction, we deposited single MXene layers on SiO_2/Si substrates of different thicknesses. The latter were prepared by etching standard Si wafers—with 285 nm thick, thermally grown SiO_2 (CrysTec, Berlin, Germany)—in buffered HF (20%) for 15, 30, 60, 90, and 120 s, which resulted in SiO_2 thicknesses of 223, 170, 134, 127, and 87 nm, respectively. To determine the SiO_2 thicknesses, a set of wafers—with a 285 nm thick thermal oxide—were etched, as above, with part of the wafer masked. A profilometer was then used to measure the step height between the etched and un-etched regions yielding the SiO_2 thickness. These measurements were confirmed by a colorimetric comparison between

the color of SiO_2 of the etched samples and the calculated ones for the measured thicknesses. To complete the set, a 90 nm thick SiO_2 layer thermally grown on Si (CrysTec Berlin, Germany) was also used.

When the TCD simulations (solid line in Figure 5(a)) and the experimental results (data points with error bars in Figure 5(a)) are compared, it is obvious that the agreement is quite good. The images were taken with a camera (Canon EOS 500D), attached to an OM (Zeiss Axiotech) with a 100 X objective and a numerical aperture of 0.75. The results (Figure 5(b–h)) are shown after luminosity balancing (full procedure for balancing and comparison between theory and experiments is discussed in the SI). The experimental results confirm that the best contrast is achieved with a SiO_2 thickness of 223 nm, where TCD peaks at ≈ 12 (Figure 5(c)) in excellent agreement with our theoretical predictions (12.3 at 222 nm). Interestingly, the second highest peak of visibility is calculated to be around 280 nm with a TCD of 11.8 (confirmed by a measured value of 11.5 at 285 nm). This thickness would allow good visibility for both MXene and graphene. It is worth noting that the thickness of every flake shown in Figure 5(b–h) was measured by AFM before observing them in the OM. Only single flakes were imaged in the OM and used.

In conclusion, making use of Fresnel's theory, we delineate the conditions under which MXene mono- and, in principle, multilayers can be rendered visible under an OM—using a W-lamp—after deposition on Si wafers with various SiO_2 thicknesses. Our simulations predict that SiO_2 thicknesses of 222 and 280 nm should result in the best contrast as observed experimentally. This work establishes a framework for detecting single MXene flakes on Si and other substrates. Colorimetric results on other substrates, such as Al_2O_3/Si, HfO_2/Si, Si_3N_4/Si and Al_2O_3/Al, with other illuminants (D65), present a shift of the maxima of contrast, but are similar in general to those on silica. For further details about these results and details of our methodology refer to the SI.

Funding

This work was funded by Ceramics Division of NSF (DMR-1310245) and Swedish Foundation for Strategic Research (Synergy Grant FUNCASE).

References

[1] Fiori G, Bonaccorso F, Iannaccone G, et al. Electronics based on two-dimensional materials. *Nat Nanotech*. 2014;9:768–779.
[2] Ferrari AC, Bonaccorso F, Fal'ko V, et al. Science and technology roadmap for graphene, related two-dimensional crystals, and hybrid systems. *Nanoscale*. 2015;7:4598–4810.
[3] Gupta A, Sakthivel T, Seal S. Recent development in 2D materials beyond graphene. *Prog Mater Sci*. 2015;73:44–126.
[4] Niu T, Li A. From two-dimensional materials to heterostructures. *Prog Surf Sci*. 2015;90:21–45.
[5] Geim AK, Grigorieva IV. Van der Waals heterostructures. *Nature*. 2013;499:419–425.
[6] Novoselov KS, Geim AK, Morozov SV, et al. Electric field effect in atomically thin carbon films. *Science*. 2004;306:666–669.
[7] Ci L, Song L, Jin C, et al. Atomic layers of hybridized boron nitride and graphene domains. *Nat Mater*. 2010;9:430–435.
[8] van der Zande AM, Huang PY, Chenet DA, et al. Grains and grain boundaries in highly crystalline monolayer molybdenum disulphide. *Nat Mater*. 2013;12:554–561.
[9] Duan X, Wang C, Pan A, et al. Two-dimensional transition metal dichalcogenides as atomically thin semiconductors: opportunities and challenges. *Chem Soc Rev*. 2015;44:8859–8876.
[10] Allain A, Kis A. Electron and hole mobilities in single-layer WSe_2. *ACS Nano*. 2014;8:7180–7185.
[11] Liu H, Du Y, Deng Y, et al. Semiconducting black phosphorus: synthesis, transport properties and electronic applications. *Chem Soc Rev*. 2015;44:2732–2743.
[12] Naguib M, Kurtoglu M, Presser V, et al. Two dimensional nanocrystals produced by exfoliation of Ti_3AlC_2. *Advan Mater*. 2011;23:4248–4253.
[13] Naguib M, Come J, Dyatkin B, et al. MXene: a promising transition metal carbide anode for lithium-ion batteries. *Electrochem Commun*. 2012;16:61–64.
[14] Mashtalir O, Naguib M, Dyatkin B, et al. Kinetics of aluminum extraction from Ti_3AlC_2 in hydrofluoric acid. *Mater Chem Phys*. 2013;139:147–152.
[15] Naguib M, Mochalin VN, Barsoum MW, et al. MXenes: a new family of two dimensional materials. *Advan Mater*. 2014;26:992–1005.
[16] Barsoum MW. *MAX: phases properties of machinable carbides and nitrides*. Weinheim: Wiley VCH GmbH & Co.; 2013.
[17] Halim J, Cook KM, Naguib M, et al. X-ray photoelectron spectroscopy of select multi-layered transition metal carbides (MXenes). *Appl Surf Sci*. 2016;362:406–417.
[18] Halim J, Kota S, Lukatskaya MR, et al. Synthesis and characterization of 2D molybdenum carbide (MXene). *Adv Funct Mater*. 2016;26:3118–3127.
[19] Liang X, Garsuch A, Nazar LF. Sulfur cathodes based on conductive MXene nanosheets for high performance lithium–sulfur batteries. *Angew Chem Inter Ed*. 2015;54:3907–3911.
[20] Er D, Li J, Naguib M, et al. Ti_3C_2 MXene as a high capacity electrode material for metal (Li, Na, K, Ca) Ion batteries. *ACS Appl Mater Interfaces*. 2014;6(14):11173–11179.
[21] Lukatskaya MR, Mashtalir O, Ren CE, et al. Cation intercalation and high volumetric capacitance of two-dimensional titanium carbide. *Science*. 2013;341:1502–1505.
[22] Ghidiu M, Lukatskaya, MR, Zhao MQ, et al. Conductive two-dimensional titanium carbide 'clay' with high volumetric capacitance. *Nature*. 2014;516:78–81.

[23] Xie X, Chen S, Ding W, et al. An extraordinarily stable catalyst: Pt NPs supported on two-dimensional $Ti_3C_2X_2$ (X = OH, F) nanosheets for oxygen reduction reaction. *Chem Comm*. 2013;49:10112–10114.
[24] Liu H, Duan C, Yang C, et al. A novel nitrite biosensor based on the direct electrochemistry of hemoglobin immobilized on MXene-Ti_3C_2. *Sensors Actuators B: Chem*. 2015;218:60–66.
[25] Chen J, Chen K, Tong D, et al. CO_2 and temperature dual responsive 'Smart' MXene phases. *Chem Comm*. 2015;51:314–317.
[26] Halim J, Lukatskaya, MR, Cook K, et al. Transparent conductive two-dimensional titanium Carbide epitaxial thin films. *Chem Mater*. 2014;26:2374–2381.
[27] Dillon AD, Ghidiu MJ, Krick AL, et al. Highly conductive optical quality solution-processed films of 2D titanium carbide. *Adv Funct Mater*. 2016;26:4162–4168.
[28] Mashtalir O, Cook KM, Mochalin VN, et al. Dye adsorption and decomposition on two-dimensional titanium carbide in aqueous media. *J Mater Chem A*. 2014;2:14334–14338.
[29] Peng Q, Guo J, Zhang Q, et al. Unique lead adsorption behavior of activated hydroxyl group in two-dimensional titanium carbide. *J Am Chem Soc*. 2014;136:4113–4116.
[30] Anasori B, Lukatskaya M, Gogotsi, Y. 2D metal carbides and nitrides (MXenes) for energy storage. *Nat Mater Rev*. doi:10.1038/natrevmats.2016.98
[31] Bhimanapati GR, Lin Z, Meunier V, et al. Recent Advances in two-dimensional materials beyond graphene. *ACS Nano*. 2015;9:11509–11539.
[32] Lei JC, Zhang X, Zhou Z. Recent advances in MXene: Preparation, properties, and applications. *Front Phys*. 2015;10:107303.
[33] Zhang H. Ultrathin Two-dimensional nanomaterials. *ACS Nano*. 2015;9:9451–9469.
[34] Miranda A, Halim J, Barsoum MW, et al. Electronic properties of freestanding $Ti_3C_2T_x$ MXene monolayers. *Appl Phys Lett*. 2016:108:033102.
[35] Blake P, Hill EW, Castro Neto AH, et al. Making graphene visible. *Appl Phys Lett*. 2007;91:063124.
[36] Jung I, Pelton M, Piner R, et al. Simple approach for high-contrast optical imaging and characterization of graphene-based sheets. *Nano Lett*. 2007;7:3569–3575.
[37] Roddaro S, Pingue P, Piazza V, et al. The optical visibility of graphene: interference colors of ultrathin graphite on SiO_2. *Nano Lett*. 2007;7:2707–2710.
[38] Ni ZH, Wang HM, Kasim J, et al. Graphene thickness determination using reflection and contrast spectroscopy. *Nano Lett*. 2007;7:2758–2763.
[39] Gao L, Ren W, Li F, et al. Total color difference for rapid and accurate identification of graphene. *ACS Nano*. 2008;2:1625–1633.
[40] Benameur MM, Radisavljevic B, Heron JS, et al. Visibility of dichalcogenide nanolayers. *Nanotech*. 2011;22:125706.
[41] Gorbachev RV, Riaz I, Nair RR, et al. Hunting for monolayer boron nitride: optical and Raman signatures. *Small*. 2011;7:465–468.
[42] Müller MR, Gumprich A, Ecik E, et al. Visibility of two-dimensional layered materials on various substrates. *J Appl Phys*. 2015;118:145305.
[43] Nemes-Incze P, Osváth Z, Kamarás K, et al. Anomalies in thickness measurements of graphene and few layer graphite crystals by tapping mode atomic force microscopy. *Carbon*. 2008;46:1435–1442.
[44] Mechler Á, Kopniczky J, Kokavecz J, et al. Anomalies in nanostructure size measurements by AFM. *Phys Rev B*. 2005;72:125407.
[45] Kühle A, Sorensen AH, Zandbergen JB, et al. Contrast artifacts in tapping tip atomic force microscopy. *Appl Phys A: Mater Sci Process*. 1998;66:S329–S332.
[46] Mechler Á, Kokavecz J, Heszler P, et al. Surface energy maps of nanostructures: atomic force microscopy and numerical simulation study. *Appl Phys Lett*. 2003;82:3740–3742.
[47] Novoselov KS, Jiang D, Schedin F, et al. Two-dimensional atomic crystals. *Proc Natl Acad Sci USA*. 2005;102:10451–10453.
[48] Cheon S, Kihm KD, Kim Hg, et al. How to reliably determine the complex refractive index (RI) of graphene by using two independent measurement constraints. *Scien Rep*. 2014;4:6364.
[49] Bruna M, Borini S. Optical constants of graphene layers in the visible range. *Appl Phys Lett*. 2009;94:031901.
[50] Herzinger CM, Johs B, McGahan WA, et al. Ellipsometric determination of optical constants for silicon and thermally grown silicon dioxide via a multi-sample, multi-wavelength, multi-angle investigation. *J Appl Phys*. 1998;83:3323–3336.
[51] Ghosh G. Dispersion-equation coefficients for the refractive index and birefringence of calcite and quartz crystals. *Opt Commun*. 1999;163:95–102.
[52] Jellison Jr G, Chisholm M, Gorbatkin S. Optical functions of chemical vapor deposited thin-film silicon determined by spectroscopic ellipsometry. *Appl Phys Lett*. 1993;62:3348–3350.
[53] Heavens OS. Optical properties of thin films. *Reports Prog Phys*. 1960;23:1.
[54] Schanda J. *Colorimetry: understanding the CIE system*. Hoboken (NJ): Wiley; 2007.